Glass Forming Ability in Pr-(Cu, Ni)-Al Alloys

Yong Zhang, Yi Li

Singapore-MIT Alliance, National University of Singapore, Singapore 119260

Abstract—**Glass forming ability (GFA) in the Pr-rich Pr-(Cu, Ni)-Al alloys at or near the eutectic points was systematically studied. It was found that the GFA in the pseudo-ternary alloys of Pr-(Cu, Ni)-Al is higher than that of the ternary alloys of Pr-Cu-Al. Two eutectic compositions in Pr-(Cu, Ni)-Al alloys were found by DSC, namely, $Pr_{68}(Cu_{0.5}Ni_{0.5})_{25}Al_7$ and $Pr_{52}(Cu_{0.5}Ni_{0.5})_{25}Al_{23}$ (at %). The later one shows better GFA than the first one. However, the best GFA was obtained at an off-eutectic composition of $Pr_{54}(Cu_{0.5}Ni_{0.5})_{30}Al_{16}$, which can be formed in fully amorphous rod with diameter of 1.5 mm by copper mould casting. The deviation of the best GFA composition from the eutectic point [$Pr_{68}(Cu_{0.5}Ni_{0.5})_{25}Al_7$] was explained in terms of the asymmetric coupled eutectic zone and the higher glass transition temperature T_g on the hypereutectic side.**

Key Words—**Bulk metallic glasses, Pr-based alloy, ternary eutectic, coupled eutectic zone.**

I. Introduction

Bulk metallic glass (BMG) is a new kind of materials compared with the conventional metallic glasses, such as ribbons and powders [1~3]. BMGs exhibit unique properties which are not found in its counterpart-crystalline materials. For example, Zr-based BMGs exhibit excellent mechanical properties [1] and Fe-based BMGs exhibit excellent magnetic properties [4]. In the past several years, many BMG forming alloys were discovered, these include $Zr_{41}Ti_{14}Cu_{12.5}Ni_{10}Be_{22.5}$ [1], $Pd_{40}Ni_{10}Cu_{30}P_{20}$ [4], $La_{55}Al_{25}Ni_5Cu_{10}Co_5$ [5], $Nd_{60}Fe_{20}Al_{10}Co_{10}$ [6], $Zr_{57}Nb_5Cu_{15.4}Ni_{12.6}Al_{10}$ [7], $Zr_{48}Nb_8Fe_8Cu_{12}Be_{24}$ [8], etc. Some principles were proposed for the discovering new BMGs [2, 4]. It is well known that the alloy with the best glass forming ability (GFA) is always at or near the eutectic point [1, 3, 5, 9], and the limitations on eutectic growth rate can promote the formation of metallic glass [10]. When the polymorphic melting curves (T_0 curve) drop steeply at the terminals of the eutectic, partitionless solidification is impossible, and interface undercooling has to become high before either solute trapping or absolute stability can appear. If the glass transition temperature (T_g) is high relative to the eutectic temperature, rapid solidification of the eutectic will ultimately produce a glass [10]. Therefore, the eutectic composition of multi-components alloy systems, with diving T_0 curves, are good candidates of BMG forming alloys.

The binary phase diagrams of Pr-Cu, Pr-Ni, and Pr-Al show eutectic with diving T_0 curves, so Pr-(Cu, Ni)-Al alloys were chosen, and the GFA at or near the eutectic was studied. Our previous work [12] has alloys. As Ni is continuously dissolvable with Cu, the eutectic of Pr-(Cu, Ni)-Al pseudo-ternary alloys was also investigated in the present study. In this paper, the locus of the best GFA composition and eutectic compositions in the ternary and pseudo-ternary phase diagrams were systematically studied. The GFA of these alloys is discussed.

II. Experimental Procedures

The master alloys were prepared by arc melting the constituent elements with purity of 99.5 wt% for Pr, 99.9 wt% for Cu, Ni and Al, respectively. The alloys were melted at least six times to ensure compositional uniformity. In this study, four cooling rate levels were used. **M**: Melt spinning onto a single copper roller with a linear velocity of 20 m/s or 30 m/s, this enables all the alloys studied can be made into fully amorphous. **C**: Chill casting by suction the melts into a copper mould. The rod samples are with length of 30 mm, and diameter of 1 mm to 3 mm; the plate samples are with length of 30 mm and width of 5 mm, and the thickness of 1 mm to 3 mm. **W**: Water quenching. The samples were sealed in quartz tube with an inner diameter of 2 mm~3 mm, heated to melting by a torch, then quenched in water. **A**: Air cooling. The samples were sealed in quartz tube with an inner diameter of 2 mm~3 mm, heated to melting by a torch, then cooled in air.

The thermal parameters, such as T_g, T_x, onset melting temperature T_m, offset melting temperature T_l were determined by differential scanning calorimeter (DSC), with a heating rate of 20 K/min. Cu pans were used and the DSC cell was purged by argon during heating. The X-ray diffraction (XRD) was performed on a Philips-PW diffractometer with Cu K_α radiation. To detect the inner part of the casting rod with diameter of 1.5 mm, about 10 rods were mounted in polymer perpendicularly, and polished, these guarantee a large flat surface to be performed by XRD. The samples were also polished and observed by Philips-FEG scanning electron microscope (SEM) in the back scattering electron (BSE) image mode and second electron (SE) mode.

The eutectic alloy has a minimum T_l and constant value of T_m compared with its surrounding alloys. This criterion was used to look for the eutectic point. The T_l and T_m values of Pr-(Cu, Ni)-Al alloys were measured by DSC.

In our study, GFA is evaluated by measuring the volume fraction (F_a) of the amorphous phase in the alloys prepared by fixed cooling rate. The samples of the same thickness of the plates or same diameter of the rods were prepared by copper mould casting to ensure the same cooling rate. The values of F_a can be evaluated by the crystallization heat measure by DSC, the first broad amorphous hump compared with the crystalline diffraction peaks measured by XRD, or the microstructure observation by SEM.

III. RESULTS

The eutectic composition in Pr-rich Pr-Cu-Al alloys ($Pr_{68}Cu_{25}Al_7$) has been confirmed in detail in Ref. [12], and the eutectic reaction can be expressed by:

$$L==Pr+PrCu+Pr_3Al$$

As Ni is continuously dissoluble with Cu, half amount of Cu is substituted by Ni, in the eutectic alloy, namely, $Pr_{68}(Cu_{0.5}Ni_{0.5})_{25}Al_7$.

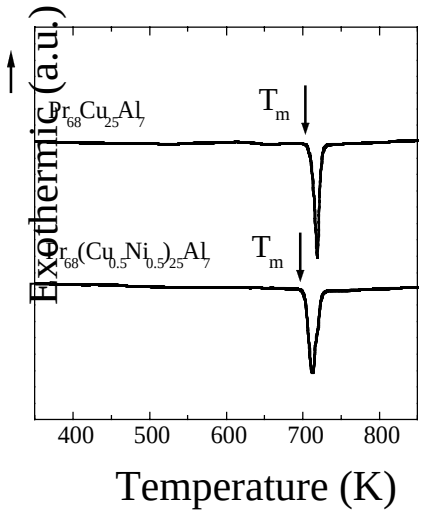

Fig.1. Melting curves of the ternary eutectic $Pr_{68}Cu_{25}Al_7$ and pseudo-ternary eutectic $Pr_{68}[Cu_{0.5}Ni_{0.5}]_{25}Al_7$ with a heating rate of 20 K/min.

Figure 1 shows the melting curves of $Pr_{68}Cu_{25}Al_7$ and $Pr_{68}(Cu_{0.5}Ni_{0.5})_{25}Al_7$ alloy ingots with a heating rate of 20 K/min. Both of the curves show a single melting peak. However, the T_l of $Pr_{68}(Cu_{0.5}Ni_{0.5})_{25}Al_7$ alloy (703 K) is slightly lower than that of the $Pr_{68}Cu_{25}Al_7$ alloy (705 K), while the melting peak of $Pr_{68}(Cu_{0.5}Ni_{0.5})_{25}Al_7$ alloy is a slightly wider than that of the $Pr_{68}Cu_{25}Al_7$ alloy, this indicates the alloy $Pr_{68}(Cu_{0.5}Ni_{0.5})_{25}Al_7$ is or very close to the pseudo-ternary eutectic. To confirm the eutectic composition of $Pr_{68}(Cu_{0.5}Ni_{0.5})_{25}Al_7$ alloy, the melting curves of the surrounding alloys along two directions were studied by DSC, as shown in Figure 2.

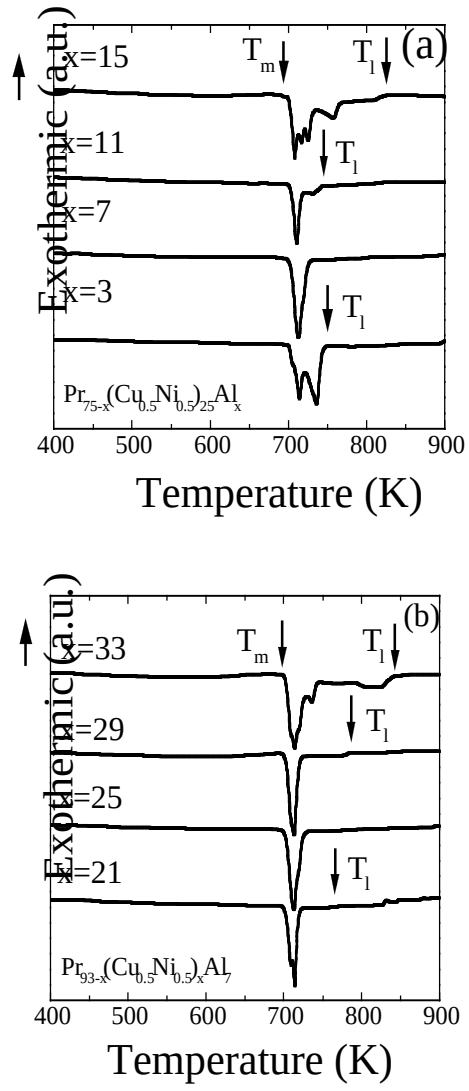

Fig.2. DSC curves of the alloys around the $Pr_{68}[Cu_{0.5}Ni_{0.5}]_{25}Al_7$ alloy with heating rates of 20 K/min. (a) $Pr_{75-x}(Cu_{0.5}Ni_{0.5})_{25}Al_x$ (x=3, 7, 11, 15); (b) $Pr_{93-x}(Cu_{0.5}Ni_{0.5})_xAl_7$ (x=21, 25, 29, 33).

Figure 2 (a) shows the melting curves of $Pr_{75-x}(Cu_{0.5}Ni_{0.5})_{25}Al_x$ (x=3, 7, 11, 15) ingots, it is apparent that the T_m stays a constant temperature and the alloys deviating from the composition of $Pr_{68}(Cu_{0.5}Ni_{0.5})_{25}Al_7$ show overlapped melting peaks and higher T_l values. Figure 2 (b) shows the melting curves of $Pr_{93-x}(Cu_{0.5}Ni_{0.5})_xAl_7$ (x=21, 25, 29, 33) ingots with a heating rate of 20 K/min, T_l also exhibits minimum at the composition of $Pr_{68}(Cu_{0.5}Ni_{0.5})_{25}Al_7$. Therefore, $Pr_{68}(Cu_{0.5}Ni_{0.5})_{25}Al_7$ alloy is or very near eutectic in thermodynamics. However, this does not guarantee eutectic microstructure.

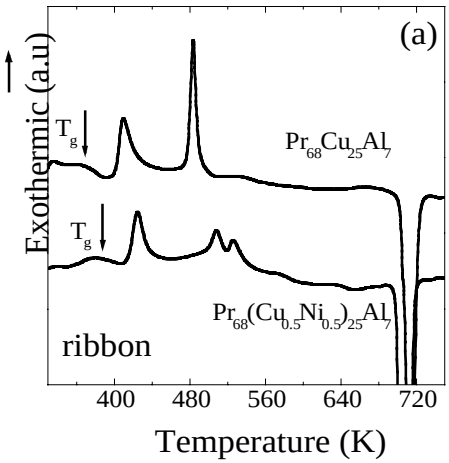

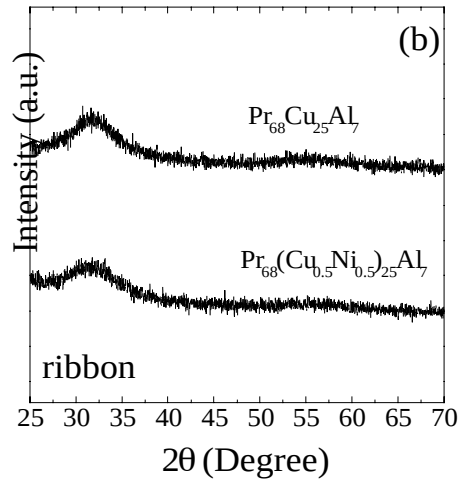

Fig.3. DSC curves at a heating rate of 20 K/min (a), and the XRD patterns (b) for the ternary eutectic $Pr_{68}Cu_{25}Al_7$ and pseudo-ternary eutectic $Pr_{68}[Cu_{0.5}Ni_{0.5}]_{25}Al_7$ prepared by melt spinning with a wheel velocity of 20 m/s (a).

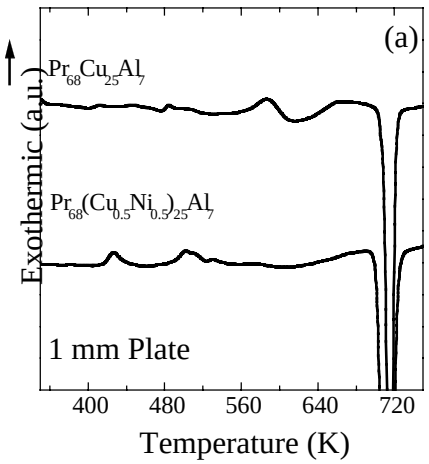

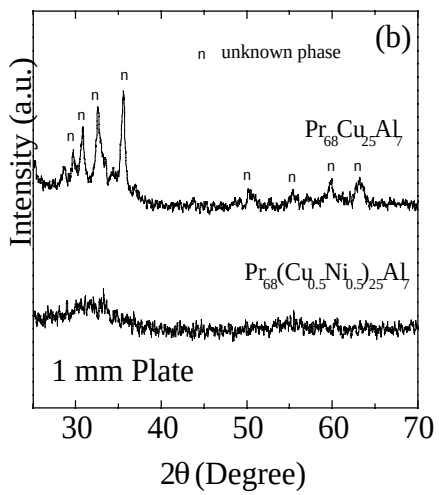

Fig.4. DSC curves at a heating rate of 20 K/min (a), and the XRD patterns (b) of the ternary eutectic $Pr_{68}Cu_{25}Al_7$ and Pseudo-ternary eutectic $Pr_{68}[Cu_{0.5}Ni_{0.5}]_{25}Al_7$ prepared by copper mould casting in to plate with 1 mm thickness.

Figure 3 shows the DSC curves [Fig. 3 (a)] and XRD patterns [Fig. 3 (b)] of the $Pr_{68}Cu_{25}Al_7$ and $Pr_{68}(Cu_{0.5}Ni_{0.5})_{25}Al_7$ alloys prepared by melt spinning with a wheel linear velocity of 20 m/s. It was found from the DSC curves [Fig 3(a)] that both the alloys exhibit distinct glass transition, the T_g values of $Pr_{68}Cu_{25}Al_7$ and $Pr_{68}(Cu_{0.5}Ni_{0.5})_{25}Al_7$ alloys are 382 K and 399 K, respectively. The first alloy exhibits a two-step crystallization process, while the later one exhibits a three-step crystallization process. This indicates that eutectic alloys cannot guarantee the crystallization from the amorphous and the supercooled liquid is eutectic. As the width of the supercooled liquid region $\Delta T_x=T_x-T_g$ is a scale of the thermal stability of the glass when heating [2], while reduced glass temperature $T_{rg}=T_g/T_l$ is a scale for the GFA[3], the measured ΔT_x, T_{rg} of $Pr_{68}Cu_{25}Al_7$ and $Pr_{68}(Cu_{0.5}Ni_{0.5})_{25}Al_7$ alloys are 20, 0.53, and 17, 0.57, respectively. That is to say the alloy $Pr_{68}(Cu_{0.5}Ni_{0.5})_{25}Al_7$ exhibits slightly weaker thermal stability and higher GFA than that of the alloy $Pr_{68}Cu_{25}Al_7$. The XRD patterns [Fig.3 (b)] show that the ribbons of the two alloys are fully amorphous, no detectable crystalline peaks were observed.

Figure 4 shows the DSC curves [Fig 4 (a)] and XRD patterns [Fig 4 (b)] of the 1 mm chill cast plate samples. Only a small crystallization peak corresponding to the second crystallization peak in the ribbon sample was observed in the $Pr_{68}Cu_{25}Al_7$ alloy with plate form, while the $Pr_{68}(Cu_{0.5}Ni_{0.5})_{25}Al_7$ alloy shows three small crystallization peaks corresponding to the three peaks of the ribbon sample, but no obvious glass transition were observed in the two alloy with plate sample. The XRD pattern of the first alloy shows many crystalline diffraction peaks (unknown phase) superimposed on the wide small amorphous peak, this indicates it

TABLE I

THE THERMAL PARAMETERS OF Pr-($Cu_{0.5}Ni_{0.5}$)-Al ALLOYS

Alloys	T_g (K)	T_x (K)	ΔT_x (K)	T_m (K)	T_l (K)	T_{rg} (K)	ΔH_m (KJ/mol)	ΔS_m (J/Kmol)	Remark.
$Pr_{68}Cu_{25}Al_7$	382	402	20	705	705	0.53	8.8	12.5	
$Pr_{72}(Cu_{0.5}Ni_{0.5})_{25}Al_3$	367	402	35	705	743	0.49	8.8	12.5	
$Pr_{72}(Cu_{0.5}Ni_{0.5})_{21}Al_7$	395	410	15	702	760	0.52	9.4	13.4	
$Pr_{68}(Cu_{0.5}Ni_{0.5})_{25}Al_7$	399	416	17	703	703	0.57	8.7	12.4	G
$Pr_{64}(Cu_{0.5}Ni_{0.5})_{29}Al_7$	416	430	14	700	786	0.53	8.9	12.7	
$Pr_{60}(Cu_{0.5}Ni_{0.5})_{33}Al_7$	428	443	15	700	843	0.51	9.2	13.1	
$Pr_{56}(Cu_{0.5}Ni_{0.5})_{37}Al_7$	445	472	27	700	886	0.50	10.0	14.3	
$Pr_{52}(Cu_{0.5}Ni_{0.5})_{41}Al_7$	457	474	17	727	919	0.50	9.3	12.8	
$Pr_{64}(Cu_{0.5}Ni_{0.5})_{25}Al_{11}$	425	440	15	703	757	0.56	8.7	12.4	
$Pr_{61}(Cu_{0.5}Ni_{0.5})_{27}Al_{12}$	437	456	19	700	803	0.54	11.4	16.3	
$Pr_{51}(Cu_{0.5}Ni_{0.5})_{37}Al_{12}$				725	934		15.8	21.8	
$Pr_{58}(Cu_{0.5}Ni_{0.5})_{28}Al_{14}$	422	480	58	700	755	0.56	8.4	12	
$Pr_{52}(Cu_{0.5}Ni_{0.5})_{34}Al_{14}$	466	500	34	721	926	0.50	12.3	17.1	
$Pr_{60}(Cu_{0.5}Ni_{0.5})_{25}Al_{15}$	444	478	34	702	819	0.54	11.9	17.0	
$Pr_{56}(Cu_{0.5}Ni_{0.5})_{29}Al_{15}$	457	509	52	707	879	0.52	8.0	11.3	
$Pr_{58}(Cu_{0.5}Ni_{0.5})_{26}Al_{16}$	454	500	46	714	821	0.55	8.4	11.8	
$Pr_{56}(Cu_{0.5}Ni_{0.5})_{28}Al_{16}$	459	518	59	710	854	0.54	11.9	16.8	
$Pr_{54}(Cu_{0.5}Ni_{0.5})_{30}Al_{16}$	466	514	48	709	880	0.53	8.7	12.3	I
$Pr_{52}(Cu_{0.5}Ni_{0.5})_{32}Al_{16}$	470	510	40	712	907	0.52	8.3	11.7	
$Pr_{50}(Cu_{0.5}Ni_{0.5})_{34}Al_{16}$	476	511	35	721	931	0.51	8.1	11.2	
$Pr_{55}(Cu_{0.5}Ni_{0.5})_{27}Al_{18}$	467	525	58	711	837	0.56	10.0	14.1	
$Pr_{50}(Cu_{0.5}Ni_{0.5})_{32}Al_{18}$	488	522	34	710	901	0.54	6.8	9.6	
$Pr_{56}(Cu_{0.5}Ni_{0.5})_{25}Al_{19}$	468	528	60	709	906	0.52	8.3	11.7	
$Pr_{57}(Cu_{0.5}Ni_{0.5})_{22}Al_{21}$	472	518	46	708	887	0.53	8.9	12.6	
$Pr_{54}(Cu_{0.5}Ni_{0.5})_{25}Al_{21}$	480	524	44	707	776	0.62	7.7	10.9	
$Pr_{58}(Cu_{0.5}Ni_{0.5})_{20}Al_{22}$	468	512	44	707	896	0.52	9.3	13.2	
$Pr_{52}(Cu_{0.5}Ni_{0.5})_{25}Al_{23}$	489	545	56	745	745	0.66	6.6	8.9	H
$Pr_{59}(Cu_{0.5}Ni_{0.5})_{17}Al_{24}$	475	506	31	746	903	0.53	9.2	12.3	
$Pr_{60}(Cu_{0.5}Ni_{0.5})_{15}Al_{25}$	480	500	20	746	920	0.52	10.7	14.3	
$Pr_{48}(Cu_{0.5}Ni_{0.5})_{25}Al_{27}$	522	559	37	751	827	0.63	5.1	6.8	

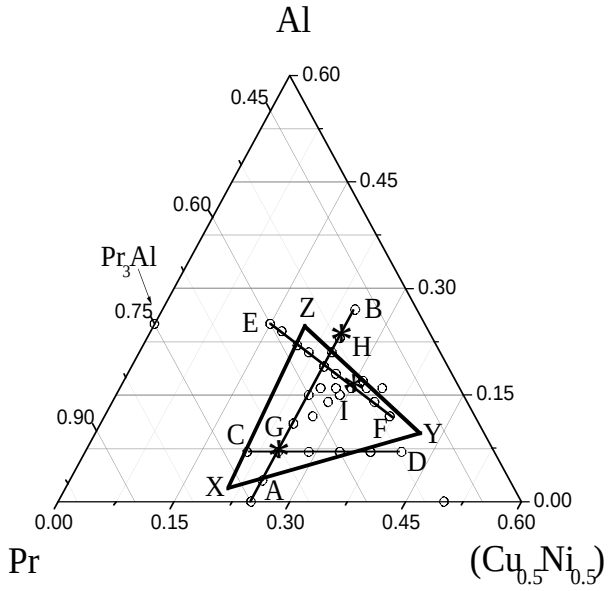

Fig.5. The alloy compositions studied in the Pr-[$Cu_{0.5}Ni_{0.5}$]-Al system, three lines were systematically studied, AB, CD, and EF. The triangle of XYZ is the eutectic horizontal plane.

contains mostly crystalline phases. The later one shows an amorphous hump with some crystalline peaks, this indicates it contains mostly amorphous. The XRD patterns are in good agreement with the DSC results. Moreover, the GFA trends are in good accordance with the T_{rg} for these two alloys. Rod samples by chill casting and other alloys near the eutectic, such as $Pr_{64}Cu_{29}Al_7$ and $Pr_{64}(Cu_{0.5}Ni_{0.5})_{29}Al_7$, also exhibit the similar trend, that is, the pseudo-ternary Pr-($Cu_{0.5}Ni_{0.5}$)-Al alloys exhibit better GFA than the ternary Pr-Cu-Al alloys. However, no fully amorphous was obtained at this pseudo-ternary eutectic point for rod sample with 1.5 mm diameter. That is to say, although the GFA of $Pr_{68}(Cu_{0.5}Ni_{0.5})_{25}Al_7$ is improved by adding Ni to the ternary $Pr_{68}Cu_{25}Al_7$ alloy, its GFA is still weak.

Figure 5 shows all the compositions studied in the pseudo-ternary Pr-($Cu_{0.5}Ni_{0.5}$)-Al alloys. In the figure, point G denotes the $Pr_{68}(Cu_{0.5}Ni_{0.5})_{25}Al_7$ eutectic point. The alloys in the triangle XYZ have the similar T_m value, indicating that they belong to the same eutectic system of G. The alloys along three main lines were studied, that is AB, CD, and EF. The compositions and the thermodynamic parameters of the studied alloys were listed in Table I. As for the GFA, point I, with composition of $Pr_{54}(Cu_{0.5}Ni_{0.5})_{30}Al_{16}$ was found having

the best GFA. Figure 6 shows the DSC heating curves [Fig. 6 (a)] and XRD patterns [Fig. 6 (b)] of the $Pr_{54}(Cu_{0.5}Ni_{0.5})_{30}Al_{16}$ alloy prepared by copper mould casting into 1.5 mm, and 2 mm diameter rods. As shown in Figure 6 (a), both rods exhibit distinct glass transitions, and a single sharp crystallization peak, and the melting shows a three steps melting process. The multi-step melting indicates that the alloy is further away from a eutectic alloy, but the DSC curves show a single and sharp crystallization peak, indicating a eutectic crystallization process. The sample of the 1.5 mm-diameter rod has higher heat of crystallization than the 2 mm one, which indicates that the former contains more amorphous phase. Figure 6 (b) shows the XRD patterns of the section of the rods with 1.5 mm and 2 mm diameters. It shows that the amorphous first hump of 1.5 mm rod is wider than the 2 mm rod, this means the first one is fully amorphous. SEM observation also verified that the 1.5 mm rod is full amorphous and 2 mm rod contains a small amount of finer crystalline phases in the inner part of the rod.

Figure 7 shows the compositional dependences of T_l, T_m, T_x, T_g, ΔT_x, and T_{rg} along the compositional lines (Fig.5.) of AB (a), CD (b), and EF (c). Figure 7 (a) shows that T_l has two minimum values at the composition of $Pr_{68}(Cu_{0.5}Ni_{0.5})_{25}Al_7$ (G) and $Pr_{52}(Cu_{0.5}Ni_{0.5})_{25}Al_{23}$ (H). The T_l isoline mapping shows both G and H points exhibit minimum, which indicate H point as well as G point, is also a eutectic. Fig.7. (a) shows both T_x and T_g increase with the Al content, and T_{rg} exhibits two maximum at the two eutectic points, while ΔT_x exhibits relatively larger values in the eutectic system of H than that of G. The higher values ΔT_x and T_{rg} in the H eutectic system indicate that the thermal stability and GFA of the alloys in the eutectic system of H are generally higher than that of eutectic system of G. This agrees well with the XRD, DSC, and SEM observation for the rod samples prepared by chill casting. Figure 7 (b) shows T_l, T_m, T_x, T_g, ΔT_x, and T_{rg} dependence on $(Cu_{0.5}Ni_{0.5})$ content along CD compositional line. The T_g and T_x increase slowly with $(Cu_{0.5}Ni_{0.5})$ content compared with Al content [Fig.7.(a)], and T_{rg} exhibits a maximum at G point. However, both T_{rg} and ΔT_x exhibit lower levels compared with AB line. The constant T_m value indicates that the alloys along the CD line, except $Pr_{52}(Cu_{0.5}Ni_{0.5})_{41}Al_7$ alloy, are in the eutectic system of G. Figure 7 (c) shows T_l, T_m, T_x, T_g, ΔT_x, and T_{rg} changing along FE compositional line. Actually, along the FE line, both Al content and $(Cu_{0.5}Ni_{0.5})$ content are changing. It shows a symmetric T_l curve, this must be an intersection of the binary eutectic line. The T_g keeps constant and T_x exhibits a maximum value at the binary eutectic point. T_{rg} and ΔT_x also exhibit maximum values at the binary eutectic line, this implies that the alloy has better GFA and thermal stability.

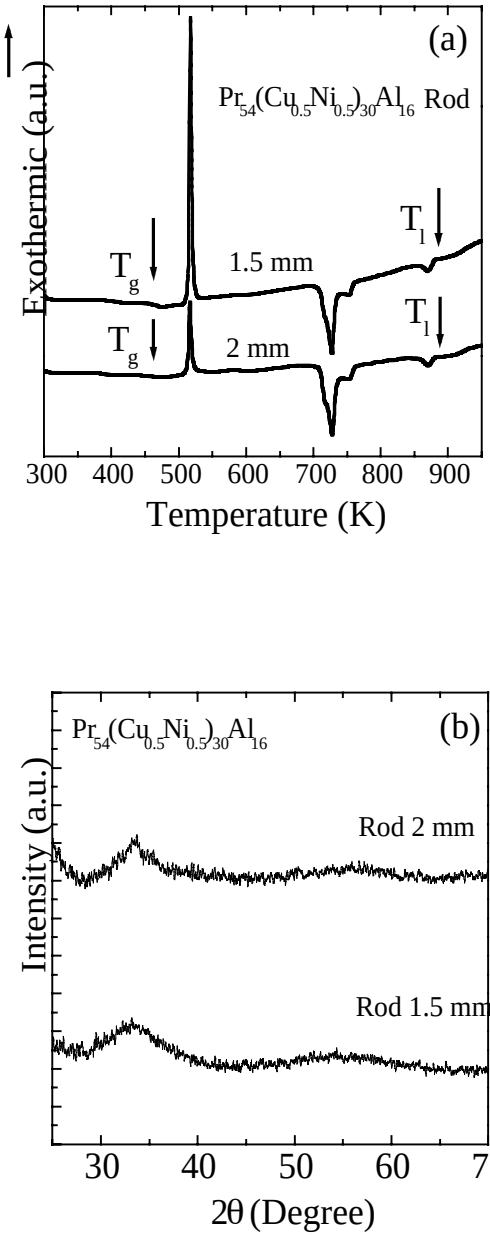

Fig.6. DSC curves (a) and XRD patterns (b) of $Pr_{54}[Cu_{0.5}Ni_{0.5}]_{30}Al_{16}$ alloy prepared by copper mould casting into 1.5 mm and 2 mm diameter rods.

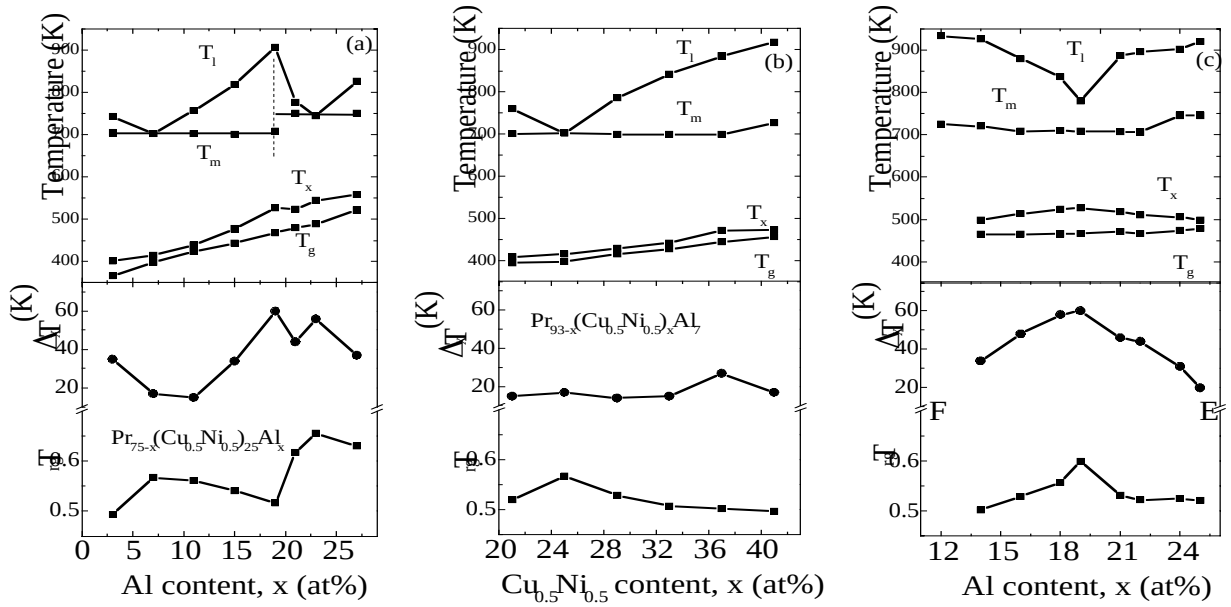

Fig. 7. The compositional dependences of T_l, T_m, T_x, T_g, T_x, and T_{rg} along the lines of AB (a), CD (b), and EF (c).

IV. DISCUSSION

Generally, T_g has a weak dependence on composition while T_l often decreases more strongly when the composition moves to eutectic. Thus, the interval between T_l and T_g generally decreases and the values of T_{rg} increase with the composition moving to eutectic [9]. However, the present work shows that T_g increases with Al and $(Cu_{0.5}Ni_{0.5})$ in eutectic system of G, and it increases more sharply with Al than with $(Cu_{0.5}Ni_{0.5})$. Chen's early works [13] had ever shown that the addition of unlike atoms always raise T_g and facilitate the formation of glasses. Therefore the higher T_g value (T_g=466 K for I point, and T_g=399 K for G point) may be one reason why the better GFA obtained at the herpyeutectic side in the eutectic system of G. On the other hand, the glass formation in the undercooled melt is a competitive process between the crystalline phases (either stable or metastable) and amorphous phase, so the morphology selection at different cooling rate is important. A schematic diagram was drawn (Fig.8.) to show the morphologies selection at different cooling rate in the eutectic system of G. The numbers 1, 2, 3, and 4 denote four alloys in the eutectic system of G, namely, $Pr_{72}(Cu_{0.5}Ni_{0.5})_{25}Al_3$, $Pr_{68}(Cu_{0.5}Ni_{0.5})_{25}Al_7$, $Pr_{64}(Cu_{0.5}Ni_{0.5})_{25}Al_{11}$, and $Pr_{54}(Cu_{0.5}Ni_{0.5})_{30}Al_{16}$. The air cooled $Pr_{68}(Cu_{0.5}Ni_{0.5})_{25}Al_7$ sample (A2) [Fig.9.(a)] shows a microstructure of cellular plus eutectic. The microstructure of the water quenched sample of $Pr_{54}(Cu_{0.5}Ni_{0.5})_{30}Al_{16}$ (W4) Doesnot exhibit eutectic morphology [Fig.9.(b)], it shows strip shaped compound like phase plus white and black phases. No eutectic microstructures were obtained for the eutectic alloy of $Pr_{68}(Cu_{0.5}Ni_{0.5})_{25}Al_7$ cooled by air (A2) or by water quenching (W2).

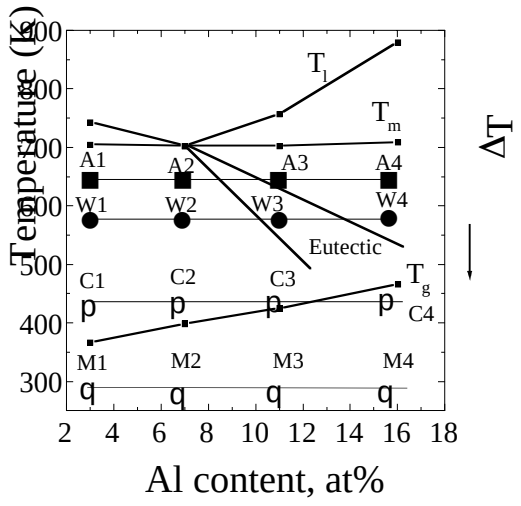

Fig. 8. Schematic diagram shows the morphologies obtained by different cooling rate, near the eutectic point. A is aircooled, W is the water quenched, C denotes copper mould casting, M denotes melt spinning

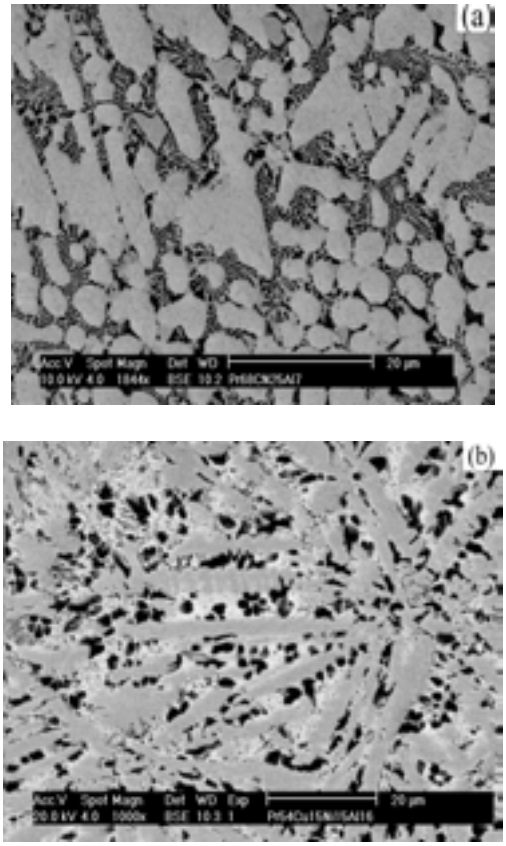

Fig.9. The microstructures of $Pr_{68}[Cu_{0.5}Ni_{0.5}]_{25}Al_7$ alloys sealed in quartz tube and cooled in air (a), and the microstructures of $Pr_{54}[Cu_{0.5}Ni_{0.5}]_{30}Al_{16}$ alloy (b) quenched in water.

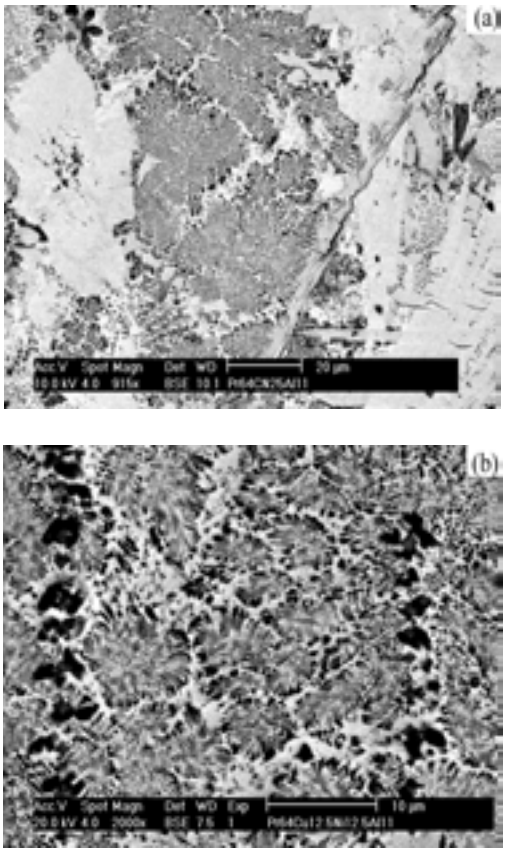

Fig.10 The microstructures of $Pr_{64}[Cu_{0.5}Ni_{0.5}]_{25}Al_{11}$ alloys sealed in quartz

However, higher volume percentage of eutectic microstructure was observed in the hypereutectic alloy $Pr_{64}(Cu_{0.5}Ni_{0.5})_{25}Al_{11}$ by air cooling [Fig.10. (a)], and the sample with water quenching (A3) shows almost fully eutectic morphology (W3) [Fig.10. (b)]. This indicates that there exists an asymmetric coupled zone toward the hypereutectic side. The skewed coupled zone is usually associated with one phase having anisotropic growth characteristics, especially for eutectic of a non-faceted phase with faceted phases, and the faceted phase can be highly undercooled [11]. Moreover, as the T_g is higher for the hypereutectic alloys, when the alloys were cooled in copper mould, the hypereutectic alloys may be cooled under T_g and transit to glass. As the cooling rate by the melt spinning is very high, so all the alloys near the eutectic can be cooled under T_g, and form a glass. The best GFA alloys deviation from eutectic has also been observed in Al-Ni-Fe-Ga alloy [14]. Kui et al [15] and Molokanov et al [16] proposed that the liquid phase separation plays an important role to modify the GFA of the eutectic. However, no traces of liquid phase separation, such as double glass transition or network microstructure, were observed near the eutectic (G) in the Pr-($Cu_{0.5}Ni_{0.5}$)-Al alloy system. Therefore, the best GFA alloy deviation from the first eutectic composition (G) is due to the skewed coupled zone and the higher value of T_g of the hypereutectic alloy.

V. Conclusions

In a summary, pseudo-ternary eutectic alloy $Pr_{68}[Cu_{0.5}Ni_{0.5}]_{25}Al_7$ exhibits better GFA than the ternary eutectic alloy $Pr_{68}Cu_{25}Al_7$. Two eutectic points were found in the Pr-$[Cu_{0.5}Ni_{0.5}]$-Al pseudo-ternary eutectic alloys, $Pr_{68}[Cu_{0.5}Ni_{0.5}]_{25}Al_7$, and $Pr_{52}[Cu_{0.5}Ni_{0.5}]_{25}Al_{23}$, the later exhibits better GFA than the former. The eutectic system of $Pr_{68}[Cu_{0.5}Ni_{0.5}]_{25}Al_7$ shows a skewed coupled zone. The best GFA composition was at $Pr_{54}[Cu_{0.5}Ni_{0.5}]_{30}Al_{16}$, bulk metallic glassy rod with diameter of 1.5 mm was formed by copper mould casting. The deviation of the best GFA composition from the eutectic point in the eutectic system of $Pr_{68}[Cu_{0.5}Ni_{0.5}]_{25}Al_7$ is due to the asymmetric coupled eutectic zone on the faceted face side and higher T_g value of the hypereutectic alloy.

Acknowledgements

The authors would like to acknowledge to the support of Singapore MIT Alliance.

References

[1] W.L. Johnson, MRS Bull., Oct., 42-56, 1995.
[2] A. Inoue, Acta mater., Vol. 48, 2000, 279-306
[3] Y. Li, Mater. Trans., Vol.42 (4), 2001, 556-561
[4] A. Inoue, A. Takeuchi, B. Shen, Mater. Trans., Vol.42 (6), 2001, 970~978.
[5] Z.P. Lu, T.T. Goh, Y. Li, S.C. NG, Acta Mater., Vol. 47 (7), 1999, 2215-2224.
[6] G.J. Fan, W. Loeser, S. Roth, J. Eckert, and L. Schultz, J. Mater. Res., Vol.15 (7), 2000, 1556~1563.
[7] C.C. Hays, J. Schroers, and W.L. Johnson, Appl. Phys. Lett., Vol.79 (11), 2001, 1605-1607
[8] Y. Zhang, D. Q. Zhao, B.C. Wei, P. Wen, M. X. Pan, W. H. Wang, J. Mater. Res. Vol.16 (6), 2001, 1675-1679.
[9] H. Tan, Z. P. Lu, H. B. Yao, Y. P. Feng, Y. Li, Mater. Trans., Vol.

[10] W.J. Boettinger: in Rapidly Solidified Amorphous and Crystalline Alloys, eds B.H. Kear, B.C. Giessen and M. Cohen, (1982), 99-102.
[11] W. Kurz, D.J. Fisher, Fundmentals of Solidification, 4Th Edition, Trans Tech Publications LTD, Switzerland. Germany, UK, USA, 1998. PP150
[12] Y. Zhang, B. Yao, H. Tan, Y. Li, J. Alloys and Compounds, in press.
[13] H.S. Chen, Acta Metallurgica, Vol.22, 1974, 1505-1511.
[14] Y. He, G.M. Dougherty, G.J. Shiflet, and S.J. Poon, Acta Metall. and Mater., Vol. 41(2), 1993, 337-343.
[15] S.Y. Hong, W.H. Guo, and H.W. Kui, J. Mater. Res., Vol. 14 (9), 1999, 3668~3672
[16] V.V. Molokanov, M.I. Petrzhik, T.N. Mikhailova, T.A. Sviridova, J. Non-Cryst. Sol., Vol. 250-252, 1999, 560-565.